Competitive Threshold Collision-Induced Dissociation: Gas-Phase Acidities and Bond Dissociation Energies for a Series of Alcohols

Vincent F. DeTuri and Kent M. Ervin*

Department of Chemistry and Chemical Physics Program, University of Nevada, Reno, Nevada 89557

Received: May 4, 1999; In Final Form: July 7, 1999

Energy-resolved competitive collision-induced dissociation methods are used to measure the gas-phase acidities of a series of alcohols (methanol, ethanol, 2-propanol, and 2-methyl-2-propanol). The competitive dissociation reactions of fluoride−alcohol, [F^-·HOR], alkoxide−water, [RO^-·HOH], and alkoxide−methanol [RO^-·$HOCH_3$] proton-bound complexes are studied using a guided ion beam tandem mass spectrometer. The reaction cross sections and product branching fractions to the two proton transfer channels are measured as a function of collision energy. The enthalpy difference between the two product channels is found by modeling the reaction cross sections near threshold using RRKM theory to account for the energy-dependent product branching ratio and kinetic shift. From the enthalpy difference, the alcohol gas-phase acidities are determined relative to the well-known values of HF and H_2O. The measured gas-phase acidities are $\Delta_{acid}H_{298}(CH_3OH) = 1599 \pm 3$ kJ/mol, $\Delta_{acid}H_{298}(CH_3CH_2OH) = 1586 \pm 5$ kJ/mol, $\Delta_{acid}H_{298}((CH_3)_2CHOH) = 1576 \pm 4$ kJ/mol, and $\Delta_{acid}H_{298}((CH_3)_3COH) = 1573 \pm 3$ kJ/mol.

I. Introduction

Bond dissociation energies of hydrocarbon molecules are of fundamental interest and are important for modeling combustion and atmospheric processes.[1−5] Ion chemistry techniques provide methods for measuring gas-phase acidities, $\Delta_{acid}H_0(RH)$, which can be related to the bond dissociation energies by use of a negative ion thermochemical cycle,[1] as shown below.

$$RH \rightarrow R^- + H^+ \qquad \Delta_{acid}H(RH)$$

$$R^- \rightarrow R + e^- \qquad EA(R)$$

$$H^+ + e^- \rightarrow H \qquad -IE(H)$$

$$RH \rightarrow R + H \qquad D(R-H) = \Delta_{acid}H(RH) + EA(R) - IE(H) \quad (1)$$

The ionization energy (IE) of hydrogen atom is known precisely, and accurate values for the electron affinity (EA) of the hydrocarbon radical can be obtained by negative ion photoelectron spectroscopy.[6]

Recently, we applied guided ion beam mass spectrometry techniques to the translational activation of bimolecular endoergic proton-transfer reactions to obtain gas-phase acidities.[7] To evaluate this method, we chose a series of alcohols whose gas-phase acidities are fairly well-known: methanol, ethanol, 2-propanol (isopropyl alcohol), and 2-methyl-2-propanol (*tert*-butyl alcohol). Reaction 2 was studied with fluoride anion as the proton-transfer reagent.

$$F^- + ROH \rightarrow RO^- + HF \qquad R = H,\ CH_3,\ CH_3CH_2,\ (CH_3)_2CH,\ \text{or}\ (CH_3)_3C \quad (2)$$

The measured 0 K reaction threshold energy for reaction 2, E_0, is an upper limit to the reaction enthalpy, Δ_rH_0, which is given by the difference between the gas-phase acidity of the alcohol and the precisely known value for HF. When comparing our results to previous literature values, we found a small systematic offset of 5−9 kJ/mol between E_0 and Δ_rH_0. There are no known intrinsic potential energy barriers along the proton-transfer reaction pathway, leading us to conclude that there are dynamical barriers to these endothermic proton reactions. Dynamical impediments to proton transfer could arise from the inability of molecular rotational energy to promote the reaction or from high curvature along the reaction path, preventing efficient translation-to-internal energy transfer with F^-. Resolution of these issues requires further study.

Because of the observed dynamical barriers to reaction 2, an alternative methodology that provides accurate gas-phase acidities is investigated here. We report energy-resolved threshold collision-induced dissociation[8] (TCID) measurements on proton-bound complexes. The TCID method enables a direct measurement of the relative gas-phase acidity between an unknown and a dissimilar reference acid. First a thermalized proton-bound $[A_1HA_2]^-$ anionic complex is formed. This complex is then collisionally excited at a controlled translational energy and can dissociate into two product channels, as shown in reaction 3 and Figure 1.

$$[A_1HA_2]^- + Xe \rightarrow A_1^- + A_2H + Xe \quad \Delta_rH_0(1) \quad (3a)$$

$$\rightarrow A_1H + A_2^- + Xe \quad \Delta_rH_0(2) \quad (3b)$$

The threshold energy difference between the two reaction channels in reaction 3 is related to the gas-phase acidity of the alcohol by eq 4.

$$\Delta E_0 = E_0(2) - E_0(1) \approx \delta\Delta_{acid}H_0 \quad (4a)$$

$$\delta\Delta_{acid}H_0 = \Delta_rH_0(2) - \Delta_rH_0(1) = \Delta_{acid}H_0(A_2H) - \Delta_{acid}H_0(A_1H) \quad (4b)$$

* Corresponding author. Electronic mail: ervin@chem.unr.edu.

10.1021/jp991459m CCC: $18.00
Published on Web 08/11/1999

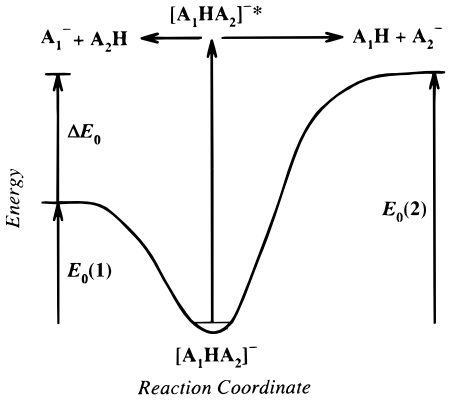

Figure 1. TCID reaction schematic for a proton-bound anionic complex.

TABLE 1: Literature Thermochemical Values for Anchor Acids (kJ/mol)

species (X−H)	EA_0 (X)	D_0 (X−H)	$\Delta_{acid}H_0$ (XH)
HO−H	176.3419 ± 0.0020[a]	494.1 ± 0.2[b]	1629.8 ± 0.2[c]
F−H	328.1649 ± 0.0004[d]	565.975 ± 0.004[e]	1549.860 ± 0.004[f]

[a] Reference 9. [b] Reference 12. [c] $\Delta_{acid}H(RH) = D(R-H) - EA(R) + IE(H)$. [d] Reference 10. [e] $D(R-H) = \Delta_{acid}H(RH) + EA(R) - IE(H)$. [f] Reference 11.

The approximation on the right-hand side of eq 4a assumes that there are no reverse activation barriers for the two dissociation channels, which is reasonable for most proton-bound complexes.[7] To extract the two threshold energies, the energy-dependent branching ratio between the two channels is modeled explicitly using the RRKM theory model developed recently by Rodgers and Armentrout.[8] The statistical unimolecular decomposition of the complex is modeled to calculate the product branching kinetics over a 1−2 eV energy range near the reaction threshold. The full statistical treatment of the dissociation pathways allows the use of proton-bound complexes of dissimilar ions. The acidities of the alcohols studied here thus can be measured directly relative to the well-defined anchor acids H_2O and HF, for which thermochemical data[9−12] are listed in Table 1. We report TCID experiments on the following systems: $A_1^- = F^-$ with $A_2H = CH_3OH$, CH_3CH_2OH, $(CH_3)_2CHOH$, and $(CH_3)_3COH$; $A_2H = H_2O$ with $A_1^- = CH_3O^-$ and $CH_3CH_2O^-$; and $A_2H = CH_3OH$ with $A_1^- = CH_3CH_2O^-$, $(CH_3)_2CHO^-$, and $(CH_3)_3CO^-$. Competitive TCID measurements on the same alcohol paired with different reference acids allow us to construct a gas-phase acidity ladder to check the internal consistency of the method. Competitive TCID is a relative method so possible errors in the absolute threshold energies appear in both product channels and should mostly cancel.

II. Experimental Section

A. Cross Section Measurements. Experiments were carried out using our guided ion beam tandem mass spectrometer, which is described in detail elsewhere.[13] Briefly, anions are created in a flow tube reactor using a microwave discharge source with helium buffer gas. $[F^-\cdot HOR]$ complexes are formed in the flow tube by making fluoride anions in the microwave discharge with hexafluorobenzene as a precursor gas, and the alcohol is introduced downstream of the microwave discharge. $[RO^-\cdot HOH]$ and $[RO^-\cdot HOCH_3]$ complexes are formed by either making HO^- or CH_3O^- in the discharge and introducing ROH downstream of the source, or by introducing both H_2O or CH_3OH and ROH downstream of the microwave discharge. All the alcohols were spectroscopic grade and used without further purification except degassing. The complexes are thermalized in the flow tube by about 2×10^5 collisions with the helium buffer gas. A magnetic sector mass spectrometer is used to select the ions of interest. After mass selection, the ions are injected into an octopole ion beam guide where they collide with xenon atoms at a controlled translational energy. Reactant and product ions are extracted from the octopole region and mass analyzed with a quadrupole mass filter and counted using an electron multiplier.

Absolute reaction cross sections are determined as a function of collision energy between the reactants; a thorough discussion has been presented previously.[13,14] The laboratory ion energy is measured using retarding potential analysis and confirmed by time-of-flight[13] and is then converted to the relative collision energy, E, in the center-of-mass frame.[14] To obtain absolute reaction cross sections under single collision conditions, the data are collected at three different pressures and the cross sections are extrapolated to zero pressure. The absolute cross section magnitudes have an estimated uncertainty of ±50%, but for two product channels relative values are within ±10%.

B. Fitting Procedure. The single-collision reaction cross section, $\sigma(E)$, is modeled with the CRUNCH[15] Fortran program using an empirical threshold law,[13,14,16] eq 5,

$$\sigma(E) = \frac{\sigma_0}{E}\sum_i g_i P_D(E,E_i,\tau)(E + E_i - E_0)^N \qquad (5)$$

where P_D is the RRKM dissociation probability discussed below, τ is the experimental time window for dissociation, E_i is the energy of reactant rovibrational state i with fractional population g_i corresponding to a Maxwell−Boltzmann distribution at 300 K, σ_0 and N are adjustable parameters, and E_0 is the 0 K reaction threshold energy. The parameter N in eq 5 defines the energy-transfer efficiency of the collision of the complex with xenon.

After collision with the xenon target gas, there is a limited time window for the energized molecule to dissociate before mass analysis and detection, resulting in a kinetic shift.[17] We correct for this kinetic shift using RRKM theory for unimolecular dissociation with an appropriate transition state model, as described by Rodgers, Ervin, and Armentrout.[16] For a CID process with two product channels, there can also be a competitive shift,[17] in which the higher energy channel is suppressed near its threshold by the presence of the more favorable channel. We use the model of Rodgers and Armentrout[8] to treat kinetic and competitive shifts in TCID, in which both channels are modeled simultaneously using RRKM theory. The detailed equations we use are presented in Appendix I. An advantage of this method is that the observed energy-dependent branching ratio between the two product channels must be reproduced, providing an internal test of the model.

The statistical dissociation is modeled assuming that the transition state is located at the centrifugal barrier with frequencies corresponding to the free fragments, i.e., we use a loose orbiting transition state model ("phase space limit"[16]). This model is appropriate since the complex is held together by ion−dipole forces and hydrogen bonding, rather than a covalent bond.[8,18] The long-range ion-induced dipole potential is calculated using the molecular polarizabilities[19] of the neutral product. Rotational constants and vibrational frequencies for the complexes and products were computed at the HF/6-31G(d) level using Gaussian 94,[20] and vibrational frequencies are scaled by 0.8953.[21] Table 2 lists the calculated frequencies for the

TABLE 2: Rotational Constants and Vibrational Frequencies (cm^{-1})[a]

	$[CH_3O^-\cdot HOH]$	$[CH_3CH_2O^-\cdot HOH]$	$[F^-\cdot HOCH_3]$
rotation	1.24, 0.16, 0.15	0.48, 0.10, 0.09	1.15, 0.20, 0.17
vibration	49, 77, 129, 285, 454, 1048, 1137,1171, 1180, 1467, 1473, 1487, 1713, 2504, 2524, 2580, 2850, 3681	26, 68, 123, 250, 306, 410, 453, 760, 826, 1023, 1036, 1172, 1174, 1266, 1352, 1396, 1454, 1466, 1497, 1715, 2515, 2563, 2794, 2861, 2887, 2905, 3683	55[b], 146, 380, 1082, 1123, 1144, 1190, 1290, 1474, 1491, 1520, 1649, 2741, 2747, 2756
	$[CH_3CH_2O^-\cdot HOCH_3]$	$[(CH_3)_2CHO^-\cdot HOCH_3]$	$[(CH_3)_3CO^-\cdot HOCH_3]$
rotation	0.42, 0.06, 0.05	0.20, 0.05, 0.04	0.14, 0.04, 0.04
vibration	26, 34, 66, 99, 139, 256, 311, 416, 762, 829, 1031, 1096, 1106, 1126, 1162, 1170, 1184, 1268, 1354, 1393, 1454, 1460, 1466, 1475, 1492, 1498, 1544, 2545, 2567, 2671, 2799, 2812, 2818, 2829, 2863, 2888	16, 30, 62, 87, 135, 230, 239, 279, 352, 412, 489, 758, 841, 871, 983, 1070, 1086, 1102, 1122, 1144, 1163, 1188, 1330, 1351, 1357, 1362, 1448, 1456, 1456, 1457, 1472, 1473, 1488, 1535, 2556, 2699, 2792, 2804, 2813, 2814, 2826, 2851, 2861, 2884, 2889	26, 39, 58, 84, 131, 218, 230, 270, 274, 322, 337, 397, 454, 478, 695, 826, 829, 899, 989, 1003, 1007, 1040, 1104, 1131, 1163, 1192, 1199, 1248, 1357, 1359, 1376, 1448, 1456, 1458, 1461, 1468, 1468, 1475, 1484, 1493, 1551, 2754, 2805, 2806, 2818, 2825, 2840, 2846, 2869, 2870, 2882, 2894, 2901, 2905
	$[F^-\cdot HOCH_2CH_3]$	$[F^-\cdot HOCH(CH_3)_2]$	$[F^-\cdot HOC(CH_3)_3]$
rotation	0.33, 0.15, 0.12	0.27, 0.09, 0.07	0.16, 0.07, 0.07
vibration	102[b], 154, 278, 345, 440, 784, 861, 1045, 1128, 1142, 1163, 1275, 1348, 1391, 1453, 1485, 1499, 1595, 1992, 2760, 2770, 2819, 2869, 2965	69[b], 138, 236, 277, 303, 340, 452, 473, 783, 885, 900, 980, 1083, 1133, 1165, 1180, 1330, 1342, 1368, 1375, 1440, 1451, 1461, 1485, 1563, 1896, 2731, 2801, 2820, 2847, 2867, 2886, 2952	105[b], 146, 228, 270, 274, 293, 329, 350, 392, 452, 498, 713, 868, 882, 928, 961, 1013, 1027, 1124, 1208, 1218, 1253, 1363, 1365, 1382, 1439, 1451, 1453, 1459, 1478, 1496, 1599, 2239, 2806, 2813, 2827, 2855, 2858, 2875, 2890, 2947, 2951

[a] From HF/6-31G(d) calculations. Calculated vibrational frequencies have been scaled by 0.8953.[21] [b] Harmonic frequency removed and treated as a hindered rotor; see Appendix II.

complexes; product molecule frequencies have been reported previously.[7] Low-frequency torsional motions can be treated as harmonic oscillators, free rotors, or hindered rotors. We treat the OH torsional motions as hindered rotors for the fluoride−alcohol complexes and dissociation products. Details of the hindered rotor treatment are given in Appendix II. Methyl rotors are treated as harmonic vibrations; because these modes appear in the complex and in both product channels, errors from this treatment will tend to cancel. No hindered rotors were considered for the alkoxide−methanol complexes or dissociation products because torsional motions are present in both product channels and will therefore largely cancel. Torsional motions in the alkoxide−water complexes were treated as harmonic vibrations, but the dissociation channel with an OH torsional motion was treated as a hindered rotor.

III. Results

A. Product Branching Ratios. Cross section results are summarized in Figures 2−4. The fluoride−alcohol complex dissociations are shown in Figure 2. The cross section of the higher energy $RO^- + HF$ product dissociation channel is at least an order of magnitude smaller than the lower energy $ROH + F^-$ channel. The alkoxide−water complex dissociations are shown in Figure 3. The gas-phase acidities of methanol and ethanol were measured relative to water. The alkoxide−methanol dissociations are shown in Figure 4.

If the $\Delta_{acid}H_0$ difference is too large, only the lower-energy decomposition channel is observed. In the dissociation of the ethoxide−water complex, the higher-energy product channel, $HO^- + CH_3CH_2OH$, is 2 orders of magnitude smaller than the lower energy channel, $H_2O + CH_3CH_2O^-$, showing the sensitivity of this technique. Isopropyl and *tert*-butyl alcohols had gas-phase acidity differences too large relative to water (>55 kJ/mol) and only the lower energy product could be observed; that is, no HO^- product was observed. Similarly, only the $F^- + H_2O$ dissociation channel was observed in TCID of the fluoride−water complex because of the large difference in gas-phase acidity between hydrogen fluoride and water, 80 kJ/mol (Table 1). These observations suggest a gas-phase acidity difference of about 50 kJ/mol is the limit of the TCID technique for these proton-bound complexes.

B. Threshold Analysis. Equation A3 is convoluted over the translational energy distribution of the reactants[14,16] and used to fit both channels simultaneously. Solid lines in Figures 2−4 show fits to the data. Table 3 lists average fitting parameters for each system, where $E_0(1) = \Delta_c H_0$ is the dissociation threshold energy for the lower energy channel and is equal to the complex dissociation energy, $\Delta E_0 = E_0(2) - E_0(1)$, and $E_0(2)$ is the dissociation threshold energy for the higher energy channel. In the nonlinear least-squares optimizations, $E_0(1)$ and ΔE_0 are treated as adjustable parameters. Because $E_0(1)$ and $E_0(2)$ are correlated, the statistical uncertainty in the relative energy is much smaller using ΔE_0 as a parameter rather than both $E_0(1)$ and $E_0(2)$. Figure 5 shows averaged 0 K relative gas-phase acidity measurements as a ladder. Values are self-consistent when compared for different pairings, demonstrating that this method can accurately measure relative gas-phase acidities between two dissimilar compounds.

The uncertainties in Table 3 for the threshold energies represent estimates of $\pm 2\sigma$. For $E_0(1)$, the uncertainties are calculated as the root-sum-of-squares of uncertainties arising from the ion energy determination (±0.05 eV lab), the statistical uncertainty in the least-squares fit to the data, the modeling error estimated by fitting different energy ranges, the uncertainties from model parameters (±20% for vibrational frequencies and factors of two for the experimental time window), and the estimated standard deviation from multiple sets of data. For ΔE_0, the ion energy uncertainty is not included because it exactly cancels and the uncertainties from molecular parameters make little difference because of cancellation in the relative threshold

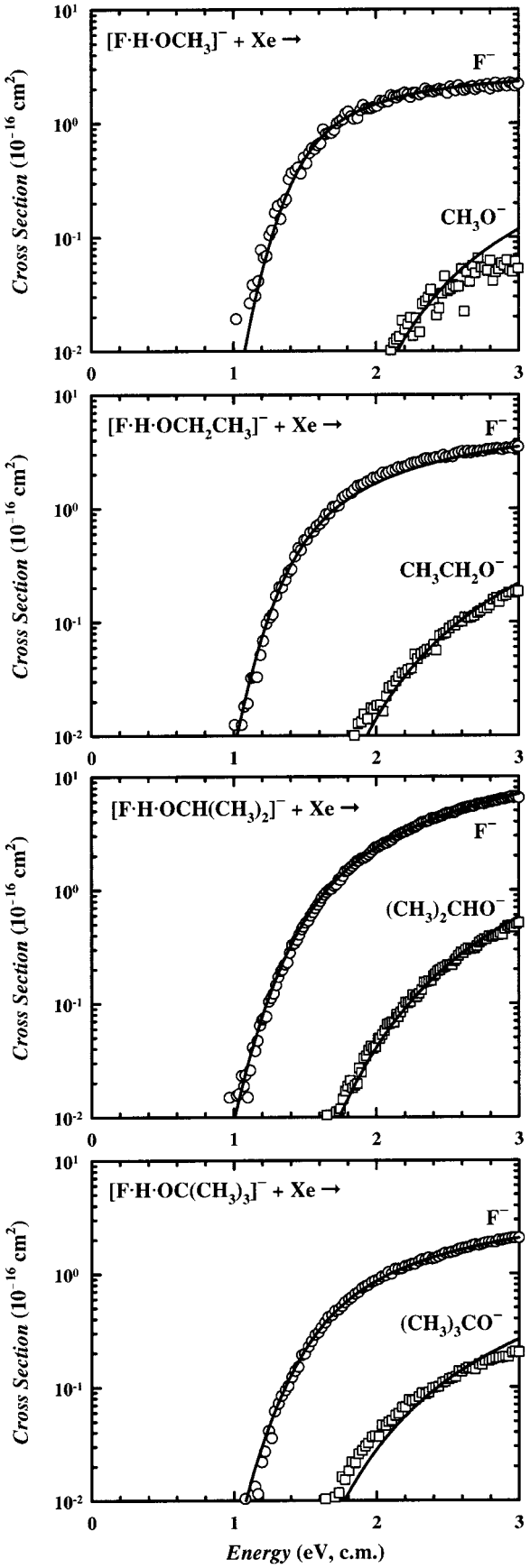

Figure 2. Single-collision cross sections for (a) $[F{\cdot}H{\cdot}OCH_3]^- \rightarrow F^- + CH_3OH$ (circles), $HF + CH_3O^-$ (squares); (b) $[F{\cdot}H{\cdot}OCH_2CH_3]^- \rightarrow F^- + CH_3CH_2OH$ (circles), $HF + CH_3CH_2O^-$ (squares); (c) $[F{\cdot}H{\cdot}OCH(CH_3)_2]^- \rightarrow F^- + (CH_3)_2CHOH$ (circles), $HF + (CH_3)_2CHO^-$ (squares); (d) $[F{\cdot}H{\cdot}OC(CH_3)_3]^- \rightarrow F^- + (CH_3)_3COH$ (circles), $HF + (CH_3)_3CO^-$ (squares). Solid lines show the fits to the data described in text.

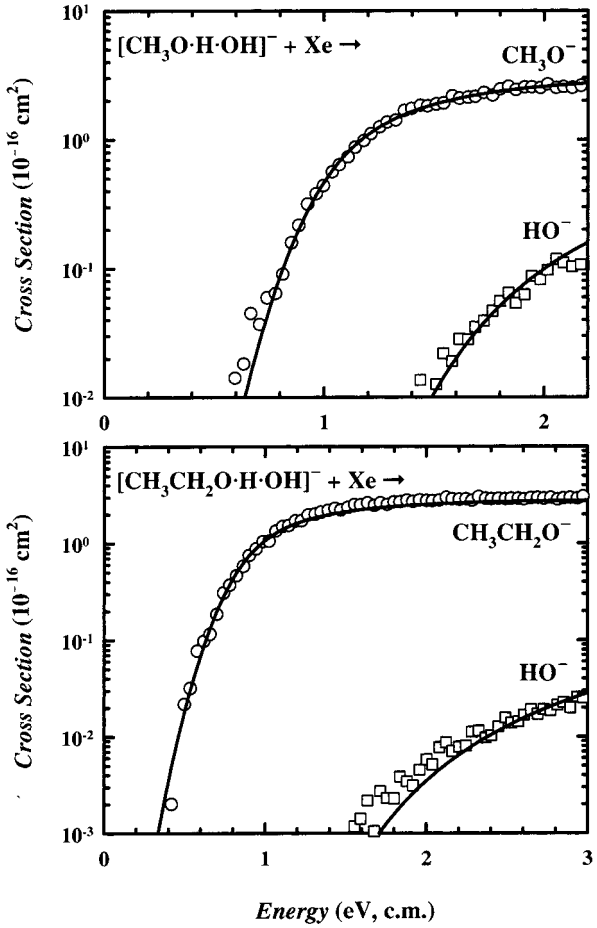

Figure 3. Single-collision cross sections for (a) $[CH_3O{\cdot}H{\cdot}OH]^- \rightarrow CH_3O^- + H_2O$ (circles), $CH_3OH + HO^-$ (squares); (b) $[CH_3CH_2O{\cdot}H{\cdot}OH]^- \rightarrow CH_3CH_2O^- + H_2O$ (circles), $CH_3CH_2OH + HO^-$ (squares). Solid lines show the fits to the data described in text.

measurement, as discussed below. The reported uncertainties do not include possible systematic errors in the threshold model.

C. Gas-Phase Acidity Determination. The absolute gas-phase acidities of the alcohols are calculated by a least-squares minimization of χ^2 from eq 6,

$$\chi^2 = \frac{\sum_{j\neq k}\left(\frac{\Delta_{acid}H_0(A_jH) - \Delta_{acid}H_0(A_kH) - \Delta E_0(j,k)}{\sigma_{j,k}}\right)^2}{\sum_{j\neq k}\left(\frac{1}{\sigma_{j,k}^2}\right)} \quad (6)$$

where $\Delta E_0(j,k) = E_0(j) - E_0(k)$ is the measured gas-phase acidity difference for the complex $[A_kHA_j]^-$, $\Delta_{acid}H_0(A_jH)$ and $\Delta_{acid}H_0(A_kH)$ are the absolute gas-phase acidities, and $\sigma_{j,k}$ is the uncertainty in the individual measurement of ΔE_0 (based on the components described above except reproducibility). The gas-phase acidities of water and hydrogen fluoride are treated as constants (Table 1), and the gas-phase acidities of the four alcohols are the adjustable parameters. The $\Delta E_0(j,k)$ values are the experimental threshold energy differences for 18 independent measurements of nine different complexes, with average values and the number of measurements for each complex listed in Table 3. The number of measurements involving each alcohol in one product channel is $v = 9$ for CH_3OH, $v = 3$ for CH_3CH_2OH, $v = 5$ for $(CH_3)_2CHOH$, and $v = 5$ for $(CH_3)_3OH$. The 95% confidence interval uncertainty for acid A_jH is

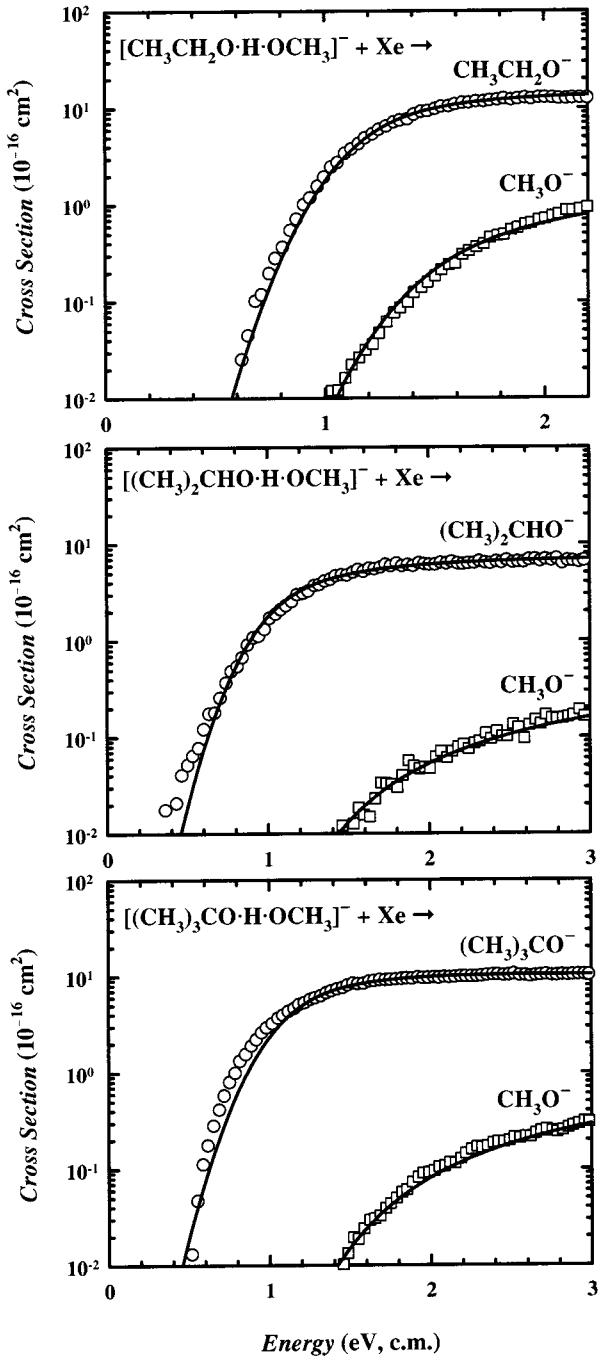

Figure 4. Single-collision cross sections for (a) $[CH_3CH_2O{\cdot}H{\cdot}OCH_3]^- \rightarrow CH_3CH_2O^- + CH_3OH$ (circles), $CH_3CH_2OH + CH_3O^-$ (squares); (b) $[(CH_3)_2CHO{\cdot}H{\cdot}OCH_3]^- \rightarrow (CH_3)_2CHO^- + CH_3OH$ (circles), $(CH_3)_2CHOH + CH_3O^-$ (squares); (c) $[(CH_3)_3CO{\cdot}H{\cdot}OCH_3]^- \rightarrow (CH_3)_3CO^- + CH_3OH$ (circles), $(CH_3)_3COH + CH_3O^-$ (squares). Solid lines show the fits to the data described in text.

calculated using eq 7, where $n = 18$ is the number of measurements, $m = 4$ is the number of adjustable parameters, and $t_{\upsilon-1,95}$ is the Student *t*-factor for $\upsilon - 1$ degrees of freedom.[22]

$$\pm\delta_j = \pm t_{\upsilon-1,95}\sigma_j = \pm t_{\upsilon-1,95}\left[\left(\frac{n}{n-m}\right)\chi^2\right]^{1/2} \qquad (7)$$

Because the individual uncertainties, $\sigma_{j,k}$, are included in eq 6, these final uncertainties take into account estimated parameters errors in the model, the reproducibility of separate experiments, and the self-consistency of the acidity ladder. This uncertainty is propagated with the uncertainties in the literature gas-phase

TABLE 3: Fitting Parameters

complex $[A_1^-{\cdot}HA_2]$	σ_0	$E_0(1)$ (eV)	ΔE_0 (eV)	N	a
$[CH_3O^-{\cdot}HOH]$	4.85	1.08 ± 0.10	0.363 ± 0.004	0.89	2
$[CH_3CH_2O^-{\cdot}HOH]$	4.45	1.04 ± 0.09	0.502 ± 0.004	0.82	1
$[CH_3CH_2O^-{\cdot}HOCH_3]$	30.7	1.11 ± 0.08	0.129 ± 0.004	0.92	1
$[(CH_3)_2CHO^-{\cdot}HOCH_3]$	11.6	0.92 ± 0.09	0.218 ± 0.004	0.83	1
$[(CH_3)_3CO^-{\cdot}HOCH_3]$	20.4	1.12 ± 0.08	0.265 ± 0.003	0.75	2
$[F^-{\cdot}HOCH_3]$	1.22	1.24 ± 0.10	0.462 ± 0.003	1.20	3
$[F^-{\cdot}HOCH_2CH_3]$	5.33	1.39 ± 0.09	0.303 ± 0.005	1.39	1
$[F^-{\cdot}HOCH(CH_3)_2]$	5.37	1.42 ± 0.09	0.215 ± 0.003	1.65	4
$[F^-{\cdot}HOC(CH_3)_3]$	2.75	1.40 ± 0.09	0.170 ± 0.003	1.62	3

[a] Number of complete data sets analyzed for each complex.

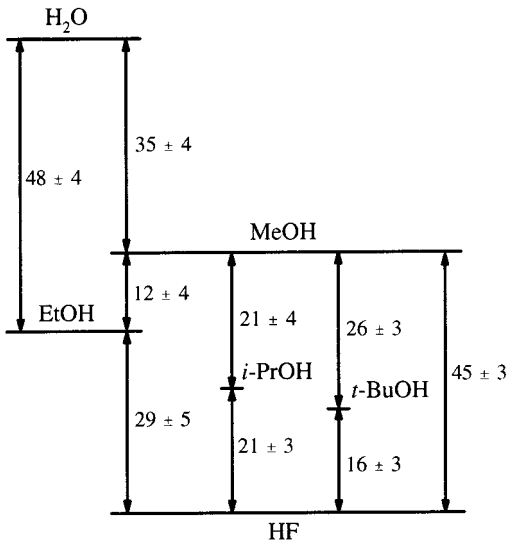

Figure 5. Relative gas-phase acidity ladder in kJ/mol.

acidities of HF and H_2O (Table 1). Table 4 summarizes the final 0 K gas-phase acidity results. The gas-phase acidity ladder can be checked by treating $\Delta_{acid}H_0(H_2O)$ as an additional adjustable parameter, with only HF as an anchor point. This results in $\Delta_{acid}H_0(H_2O) = 1628 \pm 2$ kJ/mol, in error by only −2 kJ/mol. This indicates the internal consistency of our relative gas-phase acidity measurements is within 2 kJ/mol over a range of 80 kJ/mol, i.e., within 2.5%.

D. Thermochemical Derivations. From the measured 0 K gas-phase acidities, we convert to 298 K using eq 8.

$$\Delta_r H_{298} = \Delta_r H_0 + \int_0^{298} \Delta_r C_P(T)\, dT \qquad (8)$$

From our measured enthalpies of reaction, we calculate $\Delta_{acid}G_{298}$ by eq 9.

$$\Delta_{acid}G_{298} = \Delta_{acid}H_{298} - T\Delta_{acid}S_{298} \qquad (9)$$

The $C_P(T)$ and $\Delta_{acid}S$ terms in eqs 8 and 9 are calculated by statistical mechanics in the independent vibrations−rigid rotor approximation[23] using previously reported frequencies.[7] Internal rotors are treated as harmonic oscillators except for OH torsions, which are treated as hindered rotors as described in Appendix II. Entropy values are calculated explicitly for each acid rather than the previous assumption[24] of using $\Delta_{acid}S_{298} = 92 \pm 8$ J mol^{-1} K^{-1} for all alcohols. In comparing $S_{298}(CH_3OH)$ and $S_{298}(CH_3CH_2OH)$ with previous evaluations[12] that employed more sophisticated treatments of the coupled internal rotors, our values differ by only 0.3 and 1.8 J mol^{-1} K^{-1}, respectively. Because of substantial cancellation of errors between ROH and RO^-, we estimate our $\Delta_{acid}S_{298}$ values are within 2 J mol^{-1} K^{-1} of the true value. Table 4 lists the calculated $\Delta_{acid}H_{298}$, $\Delta_{acid}S_{298}$,

TABLE 4: Gas-Phase Acidities (kJ/mol)

species	$\Delta_{acid}H_0$ TCID[b]	$\Delta_{acid}H_{298}$ TCID[c]	endoPT[d]	kinetic[e]	HPMS[f]	$\Delta_{acid}S_{298}$[a]	$\Delta_{acid}G_{298}$ TCID[g]	SIFT[h]	ICR[i]
CH_3OH	1594 ± 3	1599 ± 3	≤1605 ± 3	1595 ± 8	1597 ± 3	89 ± 2	1572 ± 3		1565 ± 8
CH_3CH_2OH	1581 ± 5	1586 ± 5	≤1592 ± 4	1582 ± 8		90 ± 2	1559 ± 5		1551 ± 8
$(CH_3)_2CHOH$	1571 ± 4	1576 ± 4	≤1587 ± 5	1572 ± 8		92 ± 2	1549 ± 4	1550 ± 3	1543 ± 8
$(CH_3)_3COH$	1568 ± 3	1573 ± 3	≤1582 ± 10	1566 ± 8		93 ± 2	1545 ± 3	1547 ± 3	1540 ± 8

[a] Gas-phase entropies calculated for this series of alcohols (J mol^{-1} K^{-1}). See text for details. [b] Threshold collision-induced dissociation, this work. [c] Conversion to 298 K using eq 8. [d] Bimolecular endothermic proton transfer.[7] Reported values are upper limits to the true gas-phase acidity. [e] Cooks kinetic method.[33] [f] High-pressure mass spectrometry.[31] [g] $\Delta_{acid}G_{298} = \Delta_{acid}H_{298} - T\Delta_{acid}S_{298}$. [h] Selected ion flow tube kinetics.[32] These values have been increased by +2 kJ/mol from the original reference based on a more recent precise measurement of D_0(HCCH).[35] [i] Ion cyclotron resonance.[24,28]

TABLE 5: RO−H Bond Dissociation Energies and RO Enthalpies of Formations (kJ/mol)

species	D_0(RO−H) TCID[a]	Δ_fH_0(RO) TCID[b]	PTS[c]	D_{298}(RO−H) TCID[d]	Δ_fH_{298}(RO) TCID	pyrolysis[e]
CH_3OH	433 ± 3	25 ± 3	28 ± 2	439 ± 3	19 ± 3	16.2
CH_3CH_2OH	434 ± 5	−1 ± 5		440 ± 5	−14 ± 5	−16.6
$(CH_3)_2CHOH$	437 ± 4	−29 ± 4		443 ± 4	−48 ± 4	−51.9
$(CH_3)_3COH$	440 ± 3	−60 ± 3		446 ± 3	−85 ± 3	−90.4

[a] This work, D_0(RO−H) = $\Delta_{acid}H_0$ + EA_0(RO) − IE_0(H). See text for details. [b] This work, Δ_fH_0(RO) = D_0(RO−H) + Δ_fH_0(ROH) − Δ_fH_0(H). [c] Photofragment translational spectroscopy[38] of $CH_3O \rightarrow CH_3 + O$. [d] Conversion from 0 to 298 K using eq 8. See text for details. [e] Recommended values from pyrolysis kinetics.[37]

TABLE 6: Enthalpies of Complexation (kJ/mol)

species $A_1^-{\cdot}HA_2$	Δ_cH_{298} TCID[a]	NIST[b]	McMahon[c]
$CH_3O^-{\cdot}H_2O$	106 ± 9	100 ± 1	
$CH_3CH_2O^-{\cdot}H_2O$	102 ± 9		
$CH_3CH_2O^-{\cdot}HOCH_3$	107 ± 8	114 ± 12	
$(CH_3)_2CHO^-{\cdot}HOCH_3$	88 ± 9		
$(CH_3)_3CO^-{\cdot}HOCH_3$	98 ± 9	107 ± 4	
$F^-{\cdot}HOCH_3$	123 ± 9	124 ± 8	
$F^-{\cdot}HOCH_2CH_3$	136 ± 9	132 ± 8	136 ± 3
$F^- \cdot HOCH(CH_3)_2$	139 ± 9	135 ± 8	140 ± 3
$F^- \cdot HOC(CH_3)_3$	137 ± 9	139 ± 8	140 ± 3

[a] This work. [b] Reference 28. [c] Reference 29.

and $\Delta_{acid}G_{298}$ values. Our previous results[7] from bimolecular endoergic proton transfer listed in Table 4 are upper limits to the true gas-phase acidity.

Table 5 summarizes the bond dissociation energy, D_0(RO−H), calculated from our gas-phase acidity measurements using eq 1 with IE(H)[25] = 1312.0496 ± 0.0010 kJ/mol and EA(RO) from recent measurements by Lineberger and co-workers.[26] The error bars in the bond dissociation energies are primarily due to our experimental gas-phase acidity results. Alkoxyl radical enthalpies of formation are calculated from eq 10 and listed in Table 5.

$$\Delta_fH(\mathrm{RO}) = D(\mathrm{RO{-}H}) + \Delta_fH(\mathrm{ROH}) - \Delta_fH(\mathrm{H}) \quad (10)$$

The enthalpies of formation of the alcohols and hydrogen atom are taken from the NIST database,[27] $\Delta_fH_{298}(CH_3OH) = -201.1 \pm 0.2$ kJ/mol, $\Delta_fH_{298}(CH_3CH_2OH) = -235.3 \pm 0.5$ kJ/mol, $\Delta_fH_{298}((CH_3)_2CHOH) = -272.3 \pm 0.9$ kJ/mol, $\Delta_fH_{298}((CH_3)_3COH) = -312.6 \pm 0.9$ kJ/mol, and $\Delta_fH_{298}(H) = 217.998 \pm 0.006$ kJ/mol. Table 6 lists complexation enthalpies for the proton-bound complexes at 298 K, calculated from $E_0(1)$ using eq 8.

IV. Discussion

A. TCID Model. This section discusses the sensitivity of the gas-phase acidities to various assumptions and parameters in the model used to fit the TCID data.

1. Kinetic and Competitive Shifts. To interpret the TCID measurements, product branching ratios for both channels must be calculated explicitly.[8] RRKM theory for unimolecular dissociation is used to calculate the dissociation rate for both channels for the energy-dependent time window. If our threshold data is fit without considering competitive dissociation (single-channel dissociation using eq A1), the extracted relative gas-phase acidities increase by 10−15 kJ/mol. This not only gives poor agreement with previous literature values, but the internal consistency of the gas phase acidity ladder is poor. Fitting the data without including the effects of a limited time window for product dissociation (i.e., no kinetic shift) increases the relative gas phase acidities by up to 25 kJ/mol. These results stress the importance of modeling the data explicitly to account for the kinetic and competitive shifts.

2. Transition State Parameters. The cross sections were modeled assuming a loose transition state (TS) because the complex is held together by electrostatic hydrogen bonding rather than a covalent bond.[8] Using a tight, fixed TS on only one product channel gives extremely poor fits to the data. Fitting both channels with a tight, fixed TS changes the relative threshold energies by −5 to +10 kJ/mol, which gives poorer internal consistency in our gas-phase acidity ladder, and also lowers the complexation energies by 5−20 kJ/mol. Table 6 compares the complexation energies from TCID measurements with literature values.[28,29] On average our results agree well and a lowering of our complexation energies by 5−20 kJ/mol would give poorer agreement, although still within mutual uncertainties for most systems. These results support the use of a loose TS to model our cross section data. Altering vibrational frequencies of the complex and the transition states by ±20% changes the relative threshold energies by ±0.5 kJ/mol (which is included in the uncertainties).

3. Reaction Degeneracy Factor. The following rotational symmetry factors were used in eq A3 to fix the reaction path degeneracies: $\sigma = 2$ for H_2O, $\sigma = 3$ for CH_3O^- and $(CH_3)_3CO^-$, and $\sigma = 1$ for all other species. Without the use of these symmetry factors, the relative gas-phase acidities shift by −10 to +10 kJ/mol, giving poorer self-consistency in the acidity ladder.

4. Scaling Factors. When modeling the competitive dissociation channels, it is possible to use a separate scaling factor for one channel as an additional adjustable parameter,[8] which acts similar to a change in reaction degeneracy. In this work, all product channels are fit without including individual channel scaling factors; that is, $\sigma_0 = \sigma_{0,1} = \sigma_{0,2}$ in eq A3. Using independent scaling factors as an additional fitting parameter, $\sigma_{0,1} \neq \sigma_{0,2}$, does of course improve the quality of some individual fits, but changes the relative threshold energies by -13 to $+2$ kJ/mol. The resulting degraded internal consistency in the gas-phase acidity ladder implies that this second scaling parameter is fitting random variation in our data, rather than correcting for deficiencies in the calculated densities of states or for instrumental detection discrimination.

5. Hindered Rotor Treatment. The torsional motions about the C−O bonds are treated as hindered rotors for the [F^-·HOR] complexes and the ROH product channel. Treatment of these hindered rotors as harmonic oscillators increases the relative threshold energies by 0.5−1 kJ/mol, which is well within our error bars. Treatment as free rotors gives lower values by 1 kJ/mol or less. Although more correct than the harmonic oscillator or free rotor treatment, the hindered rotor treatment has very little effect on the relative gas-phase acidity values. Because of this, it was not deemed necessary to use more sophisticated coupled-rotor treatments, or to employ hindered rotors for methyl group torsions that appear in both channels.

6. Reaction Temperature. The reactant ions are assumed to be thermalized to 300 K after many ($\sim 10^5$) collisions with helium buffer gas in the flow tube source. To test for the possibility of incompletely thermalized ions, we modeled the data assuming an internal ion temperature of 500 K. The extracted relative gas-phase acidities differ by only ~1 kJ/mol. However, the extracted complexation energies increase by 20−30 kJ/mol, giving poor agreement with literature complexation energies. Furthermore, we observe no metastable complex fragmentation (with no target gas), implying that our reactant ions are well thermalized.

7. Long-Range Potential. The rotational energy at the transition state, $E_R^{\ddagger}(J)$ in eq A2, is determined at the ion-induced dipole centrifugal barrier,[16] calculated using the polarizability of the neutral fragment. In reality, the neutral products formed have permanent dipole moments which could affect the long-range interaction. Klippenstein[30] modeled the [F^-·HOC(CH_3)$_3$] rates of dissociation using variational RRKM theory including the permanent dipole potential at $J = 50$ for comparison with the simpler ion-induced dipole model. Overall, this shifts the *relative* threshold energies for $k_1(E)$ and $k_2(E)$ by less than 0.2 kJ/mol, which is well within our error bars.

In summary, the competitive TCID method is extremely robust for determining relative acidities. That is, most of the errors in ΔE_0 from uncertain fitting parameters cancel when determining the relative gas-phase acidity. However, the internal consistency of our gas-phase ladder is poorer if the most complete statistical model is not used. Thus, by anchoring this series of alcohols to two well-known acids, we can determine the best fitting method for these competitive TCID measurements. Overall, the biggest deviations result when competitive or kinetic shift effects are not used in the fitting equation, which is expected. The next most important considerations for accurate relative measurements is accounting for symmetry of the dissociation products and using a reasonable TS model. Errors in treatment of the rovibrational densities of states mostly cancel since these errors are present for both dissociation channels. By comparing our complexation energies for the lower energy channel with literature values,[28,29] we provide further evidence that a loose TS model is best for proton-bound complexes and that our reactant ions are at or near 300 K. The complexation energies obtained from the absolute threshold energies are much more sensitive to model parameters than are the relative gas-phase acidities obtained from ΔE_0, as reflected in our reported uncertainties.

B. Comparison with Literature Values. Table 4 compares our competitive TCID gas-phase acidities with recent measurements reported in the literature. Our values agree well with individual equilibrium measurements from high-pressure mass spectrometry (HPMS)[31] and selected-ion flow tube kinetics (SIFT)[32] and less well with the ion cyclotron resonance (ICR) equilibria[24,28] and the Cooks kinetic method,[33,34] but still within mutual uncertainties. A complete discussion of previous literature values has been presented,[7] and a brief summary follows. The ICR equilibrium measurements give good relative gas-phase acidities, but an apparent error in the anchoring of the ICR acidity ladder results in a systematic offset of 5−8 kJ/mol. Nevertheless, our $\Delta_{acid}G_{298}$(ROH) values are within the ±8 kJ/mol error bars of the updated ICR values in the NIST database.[24,28] For methanol, our $\Delta_{acid}H_{298}$ value agrees with an independent HPMS equilibrium study[31] and our $\Delta_{acid}G_{298}$(ROH) values agree with the SIFT study,[32] which measured the acidities of 2-propanol and 2-methyl-2-propanol relative to acetylene.[7,32,35] This agreement with independent methods confirms the reliability of the competitive TCID measurements. Haas and Harrison[33] used the Cooks kinetic method to measure relative gas-phase acidity measurements of these alcohols. Since the relative measurements were calibrated against ICR equilibrium data compiled by Lias et al.,[36] their absolute acidities naturally mimic the ICR values.

Our $\Delta_f H_{298}$(RO) results are compared with pyrolysis values recommended by Batt[37] and a recent photofragment translational spectroscopy value[38] for CH_3O in Table 5. The competitive TCID measurements show good agreement with the spectroscopic value and are within 3−5 kJ/mol of the pyrolysis data.

V. Conclusions

Our relative gas-phase acidity measurements demonstrate that the competitive threshold collision-induced dissociation (TCID) method provides a well anchored gas-phase acidity ladder with good internal consistency. The well-known absolute gas-phase acidities of HF and H_2O were used as anchors. This treatment gives excellent agreement with the enthalpy of formation of CH_3O measured by photofragment translational spectroscopy[38] and with the gas-phase acidities of $(CH_3)_2CHOH$ and $(CH_3)_3$-COH measured relative to HCCH by selected ion flow tube kinetics,[32] supporting the accuracy of the TCID method. This method may be used in the future to measure unknown gas-phase acidities directly against well-known reference acids.

To interpret the reaction cross section data, product branching ratios over a 1−2 eV range are measured near the reaction threshold and modeled by RRKM theory to account for the kinetic and competitive shifts.[8,16] Because the full statistical treatment of the unimolecular dissociation kinetics is an integral and essential part of the analysis, the TCID method can be characterized as a "thermokinetic" method,[39,40] rather than as a direct threshold energy measurement. The statistical treatment allows the determination of relative gas-phase acidity measurements between dissimilar species so that most of the error results from the individual experimental uncertainties rather than the quality of the reference acid.

The new technique of threshold ion-pair production spectroscopy developed by Martin and Hepburn[11,41,42] provides direct measurements of absolute gas-phase acidities with spectroscopic precision (<1 cm^{-1}), but so far has been applied only to diatomics such as HCl and HF. For large systems, the most reliable method for obtaining relative gas-phase acidities is to measure the equilibrium constant for the proton-transfer reaction $A_1^- + A_2H \rightleftarrows A_1H + A_2^-$, but direct equilibration is not always possible for systems where one of the ions is not readily produced, the equilibrium lies far to one side, or the partial pressure measurements are problematic. Another method to bypass such problems is the Cooks kinetic method,[33,34,43] which measures the product branching ratio from metastable ion dissociation or collision-induced dissociation at one or more ion energies and assumes that the entropic factors for the two product channels are identical. This principal assumption limits the kinetic method to studying complexes with very similar structures in both product channels. The ability to measure an unknown gas-phase acidity directly against a well-known anchor acid is a primary advantage of the competitive TCID method. Also, the TCID method can measure relative gas-phase acidities of species that differ in acidity by up to 50 kJ/mol, while the kinetic method and equilibrium measurements are limited to about 10 kJ/mol in one step. The apparent precision of the kinetic method for relative acidities is better than the $\pm 3-5$ kJ/mol uncertainties reported here for TCID, but the approximations used make the actual accuracy less certain.[44] Further discussion of the Cooks kinetic method has been presented recently.[39,40,44,45]

The competitive TCID method bypasses the dynamical impediments we observed in endoergic bimolecular proton transfer. In the bimolecular proton-transfer reactions, there is a short interaction time ($\sim$1 ps) for proton transfer between the anion and the neutral. During this brief period, the anion must align with the most acidic hydrogen and deposit translational energy into the reactant coordinate. For the TCID method, a thermalized complex is formed and collisionally excited with a heavy target atom. This complex has a longer time ($\sim$100 μs) to redistribute its internal energy statistically and break the hydrogen bond, providing accurate thermochemical results.

The gas-phase acidities for this series of alcohols show that $\Delta_{acid}H$(ROH) decreases as the size of the alkyl group increases; that is, larger alkyl groups stabilize the negative charge. Similarly, the larger alkoxyl radicals have higher electron affinities due to stabilization of the anion. As discussed in early work by Brauman and co-workers,[46] anion stabilization in the gas phase is a result of the polarizability of the alkyl group. The series of bond dissociation energies for the neutral alcohols shows much less variation than the acidities, but D(RO$-$H) increases as the size of the alkyl group increases or from primary to secondary to tertiary structures. Given the small magnitude of this apparent trend, more high-precision experiments should be performed on a larger number of alcohols to determine whether size effects or structure effects are more important in the variation of bond dissociation energies.

Appendix I. Modeling Equations

This section summarizes the modeling equations used in this study, which have been previously derived.[8,16,47−49] The full specification of the integration over angular momenta of the energized complex has not been presented previously. Using the "statistical" distribution of the energized molecule rotational energies,[16] which assumes that vibrational and rotational degrees of freedom in the cluster after the collision are statistically populated, the cross section for a single-channel TCID process is given by eq A1,

$$\sigma(E) = \left(\frac{N\sigma_0}{E}\right)\sum_i g_i \int_0^{E+E_i-E_0} (\Delta E)^{N-1} \times \left(\frac{\sum_{J=0}^{J_{max}} g_J \rho_{vr}(E^* - E_R(J))(1 - \exp[-k(E^*,J;E_0)\,\tau(E)])}{\sum_{J=0}^{J_{max}} g_J \rho_{vr}(E^* - E_R(J))}\right) d(\Delta E) \quad \text{(A1)}$$

where $E^* = E + E_i - \Delta E$, $E - \Delta E$ is the energy transferred to the internal energy of the dissociating ion by collision, J is the total angular momentum after the collision, J_{max} is the maximum rotational quantum number at energy E^*, $g_J = 2J + 1$, $\rho_{vr}(E^* - E_R(J))$ is the density of rovibrational states of the energized molecule excluding the energy $E_R(J)$ in the inactive 2D external rotation, and $\tau(E)$ is the experimental time window as a function of energy approximated by $\tau(E) = l(\mu/2E)^{1/2}$, where l is the flight distance from the gas cell to the mass spectrometer. The parameters σ_0, E_0, and N are the same as defined for eq 5. The rovibrational density of states is calculated using the Beyer−Swinehart Stein−Rabinovitch direct count algorithm.[50−52] The RRKM dissociation rate coefficient,[53,54] $k(E^*, J; E_0)$, is given by eq A2,

$$k(E^*,J;E_0) = \frac{sN_{vr}^{\ddagger}(E^* - E_R^{\ddagger}(J) - E_0)}{h\rho_{vr}(E^* - E_R(J))} \quad \text{(A2)}$$

where $s = \sigma/\sigma^{\ddagger}$ is the overall reaction degeneracy for a given product channel, $N_{vr}^{\ddagger}(E)$ is the sum of states at the transition state configuration, and h is Planck's constant. The treatment of rotational effects has been described previously.[16] To model the energy-resolved competitive collision-induced dissociation cross section,[8] an additional term for the branching ratio is included as shown in eq A3.

$$\sigma_k(E) = \left(\frac{N\sigma_{0,k}}{E}\right)\sum_i g_i \int_0^{E+E_i-E_{0,k}} (\Delta E)^{N-1} \times \left(\frac{\sum_{J=0}^{J_{max}} g_J \rho_{vr}(E^* - E_r(J))[f_k(E^*,J)]}{\sum_{J=0}^{J_{max}} g_J \rho_{vr}(E^* - E_r(J))}\right) d(\Delta E) \quad \text{(A3)}$$

The parameters in eq A3 are the same as in eq A1, except f_k is the individual detection probability of product channel k given

TABLE 7: Hindered Rotor Parameters[a]

	ROH					ROHF$^-$				
R	V_0 (kJ/mol)	I (amu Å^2)	σ	n	ν (cm^{-1})	V_0 (kJ/mol)	I (amu Å^2)	σ	n	ν (cm^{-1})
CH_3	4.4	0.68	3	3	288	1.2	3.1	3	3	71
CH_3CH_2	5.7	0.84	1	3	268	9.5	27.9	1	2	44
$(CH_3)_2CH$	5.5	0.86	1	3	284	8.9	43.4	1	3	48
$(CH_3)_3C$	5.2	0.87	3	3	278	8.8	54.8	3	3	45

[a] V_0 is the height of the highest barrier relative to the lowest energy minimum, I is the reduced moment of inertia, σ is the symmetry of the rotor, n is the periodicity of the potential, and ν is the effective harmonic frequency for the bottom of the torsional well.

by eqs A4 and A5, where $k_{max} = 2$ for two product channels.

$$f_k(E^*,J) = \frac{k_k(E^*,J;E_{0,k})}{k_{tot}(E^*,J;E_{0,k})}(1 - \exp[-\tau(E)k_{tot}(E^*,J;E_{0,k})]) \quad \text{(A4)}$$

$$k_{tot}(E^*,J;E_{0,k}) = \sum_{k=1}^{k_{max}} k_k(E^*,J;E_{0,k}) \quad \text{(A5)}$$

The entire dissociation probabilities, not just the rate constants, are averaged over the J distributions in eq A1 and A3, a correction from eq 10 of Rodgers, Ervin, and Armentrout.[13] To account for deficiencies in the transition state model or detector discrimination effects, individual scaling parameters are introduced[8] in eq A3 for the two channels, $\sigma_{0,1}$ and $\sigma_{0,2}$. Without this empirical correction, $\sigma_0 = \sigma_{0,1} = \sigma_{0,2}$. Test calculations employing scaling factors for the individual rates k_k instead of outside the integrations over the E, J distributions gave nearly identical results.

Appendix II. Hindered Rotor Treatment

Hindered rotor energy levels for the torsions are calculated using a $V(\phi) = (V_0/2)(1 - \cos n\phi)$ potential, where V_0 is the barrier height and n is the periodicity of the rotor. Eigenvalues are calculated by solving the one-dimensional Schrödinger's equation with a free rotor basis set, as described by Spangler.[55] The calculated hindered rotor energy levels are folded into the Beyer−Swinehart density of states by the Stein−Rabinovitch method.[50−52] The heat capacities and entropies are determined via direct summation of the partition functions over the energy levels.

The reduced moment of inertia and the barrier heights for the hindered rotors are calculated using the methods described by East and Radom.[56] Eclipsed and staggered geometries are optimized at the MP2/6-31G(d) level fixing only the R_aC-OH (R_a = H or CH_3) dihedral angle, shown below.

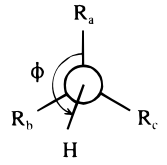

At the lowest energy minimum, the moment of inertia of each rotating group is computed about the axis containing the twisting bond. The reduced moment of inertia is approximated using configuration (2,1) in the notation of East and Radom.[56] The barrier to rotation, V_0, is calculated using MP2/6-311+G(2df,-2p) single-point energies at the MP2/6-31G(d) geometry. Table 7 gives the barrier height for the hindered rotor, the reduced moment of inertia, the symmetry of the rotor, and the harmonic frequency at the bottom of the well.

The structure above shows the torsional angle, ϕ, relative to functional groups looking along the C−O bond. For the $\sigma = 3$ rotors where $R_a = R_b = R_c$, the energy minimum is staggered (ϕ = 60, 180, and 300) and the barrier is eclipsed (ϕ = 0, 120, and 240). Ethanol, where $R_a = CH_3$ and $R_b = R_c = H$, has a minimum energy at $\phi = 180$, a barrier to hindered rotation at $\phi = 120$ and 240, a slightly higher minimum at $\phi = 60$ and 300, and the highest barrier to internal rotation at $\phi = 0$. The fluoride−ethanol complex (with H replaced by HF in the structure) has minima at $\phi = 60$ and 300, a barrier to rotation at $\phi = 180$, and a higher barrier at $\phi = 0$. This is best explained by an attractive interaction between the fluoride and the hydrogens R_b and R_c leading to a minimum, but by a large repulsion when HF eclipses the methyl group. For 2-propanol, where $R_a = R_b = CH_3$ and $R_c = H$, minima occur at $\phi = 180$ and 300, a slightly higher minimum at $\phi = 60$, and barriers at $\phi = 0$, 120, and 240. The fluoride-2-propanol complex shows minima at $\phi = 180$ and 300, a slightly higher minimum at $\phi = 60$, a barrier at $\phi = 240$, and the highest barriers at $\phi = 0$ and 120. Adding the fluoride greatly increases the moments of inertia and slightly increases the barriers to free rotation, except for the case of methanol where the barrier to free rotation is reduced. When calculating hindered rotor energy levels, the highest energy barrier to internal rotation is chosen for the barrier height. In the final fitting procedure, altering the barrier height by 50% changes the relative energy difference by no more than 0.1 kJ/mol.

Acknowledgments. We thank Professor Stephen J. Klippenstein for providing test RRKM rate calculations, Dr. James T. Vivian for furnishing Fortran code for calculating hindered rotor energy levels, and Professor W. Carl Lineberger for providing electron affinities before publication. The help of Ovette Villavicencio, supported by the NSF-REU program, is appreciated. This research is supported by the Department of Energy, Basic Energy Sciences, Grant DE-FG03-97ER14750. Partial support for V.F.D. by the Jerry and Betty Wilson Award is gratefully acknowledged.

References and Notes

(1) Berkowitz, J.; Ellison, G. B.; Gutman, D. *J. Phys. Chem.* **1994**, *98*, 2744−2765.

(2) Tsang, W. In *Energetics of Organic Free Radicals*; Simões, J. A., Greenberg, A., Liebman, J. F., Eds.; Blackie Academic and Professional: London, 1996; pp 22−58.

(3) Liñán, A.; Williams, F. A. *Fundamental Aspects of Combustion*; Oxford University Press: New York, 1993.

(4) Haynes, B. S. In *Fossil Fuel Combustion: A Source Book*; Bartok, W., Sarofim, A. F., Eds.; John Wiley & Sons: New York, 1991; pp 261−326.

(5) Filby, W. G. In *Chemical Kinetics of Small Organic Radicals*; Alfassi, Z. B., Ed.; CRC Press: Boca Raton, FL, 1988; pp 31−58.

(6) Ervin, K. M.; Lineberger, W. C. In *Advances in Gas-Phase Ion Chemistry*; Adams, N. G., Babcock, L. M., Eds.; JAI: Grenwich, CT, 1992; Vol. 1, pp 121−166.

(7) DeTuri, V. F.; Su, M. A.; Ervin, K. M. *J. Phys. Chem. A* **1999**, *103*, 1468−1479.

(8) Rodgers, M. T.; Armentrout, P. B. *J. Chem. Phys.* **1998**, *109*, 1787−1800.

(9) Schulz, P. A.; Mead, R. D.; Jones, P. L.; Lineberger, W. C. *J. Chem. Phys.* **1982**, *77*, 1153−1165.
(10) Blondel, C.; Cacciani, P.; Delsart, C.; Trainham, R. *Phys. Rev. A* **1989**, *40*, 3698−3701.
(11) Martin, J. D. D. Ph.D. Dissertation, University of Waterloo, 1998. Reported ion-pair production energy: $D_0(H^+-F^-) = 129558.2 \pm 0.3\ cm^{-1}$.
(12) *Thermodynamic Properties of Individual Substances*, 4th ed.; Gurvich, L. V., Veyts, I. V., Alcock, C. B., Eds.; Hemisphere Publishing Corporation: New York, 1989; Vol. 1.
(13) DeTuri, V. F.; Hintz, P. A.; Ervin, K. M. *J. Phys. Chem. A* **1997**, *101*, 5969−5986.
(14) Ervin, K. M.; Armentrout, P. B. *J. Chem. Phys.* **1985**, *83*, 166−189.
(15) Armentrout, P. B.; Ervin, K. M. *CRUNCH*; Fortran program.
(16) Rodgers, M. T.; Ervin, K. M.; Armentrout, P. B. *J. Chem. Phys.* **1997**, *106*, 4499−4508.
(17) Chupka, W. A. *J. Chem. Phys.* **1959**, *30*, 191−211.
(18) Spasov, V. A.; Lee, T.-H.; Maberry, J. P.; Ervin, K. M. *J. Chem. Phys.* **1999**, *110*, 5208−5217.
(19) *CRC Handbook of Chemistry and Physics*, 78th ed.; Linde, D. R., Ed.; CRC Press: New York, 1997.
(20) Frisch, M. J.; Trucks, G. W.; Schlegel, H. B.; Gill, P., et al. *Gaussian94*, revision D.4; Gaussian, Inc.: Pittsburgh, PA, 1995.
(21) Scott, A. P.; Radom, L. *J. Phys. Chem.* **1996**, *100*, 16502−16513.
(22) Skoog, D. A.; West, D. M.; Holler, F. J. *Analytical Chemistry: An Introduction*, 6th ed.; Saunders College Publishing: Philadelphia, 1994; p 91.
(23) Herzberg, G. *Molecular Spectra and Molecular Structure II. Infrared and Raman Spectra of Polyatomic Molecules*; Van Nostrand Reinhold: New York, 1945.
(24) Bartmess, J. E.; Scott, J. A.; McIver, R. T., Jr. *J. Am. Chem. Soc.* **1979**, *101*, 6046−6056.
(25) Chase, M. W., Jr. NIST-JANAF Thermochemical Tables, 4th ed. *J. Phys. Chem. Ref. Data* **1998** (Monograph No. 9).
(26) Ramond, T. M.; Schwartz, R. L.; Davico, G. E.; Lineberger, W. C. University of Colorado, Boulder, personal communication, 1999. Reported electron affinities: $EA_0(CH_3O) = 1.572 \pm 0.004$ eV, $EA_0(CH_3CH_2O) = 1.712 \pm 0.004$ eV, $EA_0((CH_3)_2CHO) = 1.847 \pm 0.004$ eV, $EA_0((CH_3)_3CO) = 1.909 \pm 0.004$ eV.
(27) Afeefy, H. Y.; Liebman, J. F.; Stein, S. E. Neutral Thermochemical Data. In *NIST Chemistry WebBook, NIST Standard Reference Database Number 69*; Mallard, W. G., Linstrom, P. J., Eds.; National Institute of Standards and Technology: Gaithersburg, MD, 1998 (http://webbook.nist.gov).
(28) Bartmess, J. E. Negative Ion Energetics Data. In *NIST Chemistry WebBook, NIST Standard Reference Database Number 69*; Mallard, W. G., Linstrom, P. J., Eds.; National Institute of Standards and Technology: Gaithersburg, MD, Nov. 1998 (http://webbook.nist.gov).
(29) Bogdanov, B.; Peschke, M.; Tonner, D. S.; Szulejko, J. E.; McMahon, T. B. *Int. J. Mass Spectrom.* **1999**, *185/186/187*, 707−725.
(30) Klippenstein, S. J. Case Western Reserve University, personal communication, 1998.
(31) Meot-Ner (Mautner), M.; Sieck, L. W. *J. Phys. Chem.* **1986**, *90*, 6687−6690.
(32) Ervin, K. M.; Gronert, S.; Barlow, S. E.; Gilles, M. K.; Harrison, A. G.; Bierbaum, V. M.; DePuy, C. H.; Lineberger, W. C.; Ellison, G. B. *J. Am. Chem. Soc.* **1990**, *112*, 5750−5759.
(33) Haas, M. J.; Harrison, A. G. *Int. J. Mass Spectrom. Ion Processes* **1993**, *124*, 115−124.
(34) Boand, G.; Houriet, R.; Gäumann, T. *J. Am. Chem. Soc.* **1983**, *105*, 2203−2206.
(35) Mordaunt, D. H.; Ashfold, M. N. *J. Chem. Phys.* **1994**, *101*, 2630−2631.
(36) Lias, S. G.; Bartmess, J. E.; Liebman, J. F.; Holmes, J. L.; Levin, R. D.; Mallard, W. G. Gas-Phase Ion and Neutral Thermochemistry. *J. Phys. Chem. Ref. Data* **1988**, *17* (Suppl. 1).
(37) Batt, L. *Int. Rev. Phys. Chem.* **1987**, *6*, 53−90.
(38) Osborn, D. L.; Leahy, D. J.; Ross, E. M.; Neumark, D. M. *Chem. Phys. Lett.* **1995**, *235*, 484−489.
(39) Armentrout, P. B. *J. Mass Spectrom.* **1999**, *34*, 74−78.
(40) Cooks, R. G.; Koskinen, J. T.; Thomas, P. D. *J. Mass Spectrom.* **1999**, *34*, 85−92.
(41) Martin, J. D. D.; Hepburn, J. W. *Phys. Rev. Lett.* **1997**, *79*, 3154−3157.
(42) Martin, J. D. D.; Hepburn, J. W. *J. Chem. Phys.* **1998**, *109*, 8139−8142.
(43) Cooks, R. G.; Wong, P. S. H. *Acc. Chem. Res.* **1998**, *31*, 379−386.
(44) Ervin, K. M. *Int. J. Mass Spectrom.*, submitted.
(45) Holmes, J. L.; Aubry, C.; Mayer, P. M. *J. Phys. Chem. A* **1999**, *103*, 705−709.
(46) Brauman, J. I.; Blair, L. K. *J. Am. Chem. Soc.* **1970**, *92*, 5986−5992.
(47) Khan, F. A.; Clemmer, D. E.; Schultz, R. H.; Armentrout, P. B. *J. Phys. Chem.* **1993**, *97*, 7978−7987.
(48) Schultz, R. H.; Crellin, K. C.; Armentrout, P. B. *J. Am. Chem. Soc.* **1991**, *113*, 8590−8601.
(49) Dalleska, N. F.; Honma, K.; Sunderlin, L. S.; Armentrout, P. B. *J. Am. Chem. Soc.* **1994**, *116*, 3519−3528.
(50) Beyer, T. S.; Swinehart, D. F. *Commun. ACM* **1973**, *16*, 379.
(51) Stein, S. E.; Rabinovitch, B. S. *J. Chem. Phys.* **1973**, *58*, 2438−2445.
(52) Stein, S. E.; Rabinovitch, B. S. *Chem. Phys. Lett.* **1977**, *49*, 183−188.
(53) Gilbert, R. G.; Smith, S. C. *Theory of Unimolecular and Recombination Reactions*; Blackwell Scientific: Boston, 1990.
(54) Baer, T.; Hase, W. L. *Unimolecular Reaction Dynamics: Theory and Experiments*; Oxford University Press: New York, 1996.
(55) Spangler, L. H. *Annu. Rev. Phys. Chem.* **1997**, *48*, 481−510.
(56) East, A. L. L.; Radom, L. *J. Chem. Phys.* **1997**, *106*, 6655−6674.